



HAL
open science

Impact of contact data resolution on the evaluation of interventions in mathematical models of infectious diseases

Diego Andrés Contreras, Elisabetta Colosi, Giulia Bassignana, Vittoria Colizza, Alain Barrat

► To cite this version:

Diego Andrés Contreras, Elisabetta Colosi, Giulia Bassignana, Vittoria Colizza, Alain Barrat. Impact of contact data resolution on the evaluation of interventions in mathematical models of infectious diseases. *Journal of the Royal Society Interface*, 2022, 19 (191), 10.1098/rsif.2022.0164 . hal-03701541

HAL Id: hal-03701541

<https://hal.science/hal-03701541>

Submitted on 22 Jun 2022

HAL is a multi-disciplinary open access archive for the deposit and dissemination of scientific research documents, whether they are published or not. The documents may come from teaching and research institutions in France or abroad, or from public or private research centers.

L'archive ouverte pluridisciplinaire **HAL**, est destinée au dépôt et à la diffusion de documents scientifiques de niveau recherche, publiés ou non, émanant des établissements d'enseignement et de recherche français ou étrangers, des laboratoires publics ou privés.



Distributed under a Creative Commons Attribution 4.0 International License

Impact of contact data resolution on the evaluation of interventions in mathematical models of infectious disease

Diego Andrés Contreras¹, Elisabetta Colosi², Giulia Bassignana², Vittoria Colizza^{2,3},
and Alain Barrat^{1,3}

¹Aix Marseille Univ, Université de Toulon, CNRS, CPT, Turing Center for Living Systems, Marseille, France

²INSERM, Sorbonne Université, Pierre Louis Institute of Epidemiology and Public Health, Paris, France

³Tokyo Tech World Research Hub Initiative (WRHI), Tokyo Institute of Technology, Tokyo, Japan

May 5, 2022

Abstract

Computational models offer a unique setting to test strategies to mitigate the spread of infectious diseases, providing useful insights to applied public health. To be actionable, models need to be informed by data, which can be available at different levels of detail. While high resolution data describing contacts between individuals are increasingly available, data gathering remains challenging, especially during a health emergency. Many models thus use synthetic data or coarse information to evaluate intervention protocols. Here, we evaluate how the representation of contact data might affect the impact of various strategies in models, in the realm of COVID-19 transmission in educational and work contexts. Starting from high resolution contact data, we use detailed to coarse data representations to inform a model of SARS-CoV-2 transmission and simulate different mitigation strategies. We find that coarse data representations estimate a lower risk of super-spreading events. However, the rankings of protocols according to their efficiency or cost remain coherent across representations, ensuring the consistency of model findings to inform public health advice. Caution should be taken, however, on the quantitative estimations of those benefits and costs triggering the adoption of protocols, as these may depend on data representation.

1 Introduction

Computational models and numerical simulations are essential tools for the understanding of epidemic spread [1, 2], at scales ranging from global to local [3, 4, 5, 6]. They have been used in the past to examine pandemic scenarios, and more extensively during the current COVID-19 pandemic, to evaluate the potential impact of non-pharmaceutical interventions (NPIs) ranging from international travel restrictions [5, 4, 7, 8, 9] to lockdowns or curfews aiming at reducing global mobility and interactions [10, 11, 12, 13], to more targeted measures such as isolation of positive cases, contact tracing, telework, partial closures of schools or surveillance by regular testing [14, 15, 16, 17, 18, 19, 20, 21, 22].

Epidemic models of infectious diseases rely both on the disease progression within hosts and on the description of how the disease can propagate from host to host, i.e., of the interactions between hosts. These interactions can be described at various levels of detail: at the coarsest level, homogeneous mixing [1] assumes that individuals potentially interact with others in a uniform way; contact matrices divide individuals into classes, and give the average duration of contacts between individuals of given

40 classes [23]; contact networks describe specifically which pairs of hosts are in contact [24, 25, 26].
41 Regardless of the level of description chosen, a model needs to be informed by data in order to be
42 actionable, i.e., to provide scenarios that can inform public health decisions. These data are typically
43 collected by surveys or diaries [27, 28, 23, 29] or, more recently, using wearable sensors able to detect
44 close-range proximity between individuals with high spatial and temporal resolution [30, 31, 32, 33, 34].

45 Gathering data is however expensive, time-consuming and implies logistical challenges, which be-
46 come particularly prohibitive for large-scale populations or multiple coupled settings, especially for
47 high-resolution data [25, 35]. The question of how much detail should be included in computational
48 models arises therefore naturally [28, 6, 36]. For instance, the estimation of superspreading events
49 needs to be informed by the heterogeneity of contact patterns [37]. Coarse representations can also
50 yield higher estimates of epidemic risk and attack rates of specific groups than more detailed repre-
51 sentations [6, 38, 39], even if a rescaling of parameters can enhance the accuracy of models based on a
52 homogeneous mixing hypothesis [40]. To overcome the limitations of coarse representations, interme-
53 diate data representations informed by statistical heterogeneities of contact numbers and durations,
54 and yielding a good estimation of the epidemic risk, have been put forward [38, 39].

55 Although data with a limited resolution were shown to be insufficient to inform interventions at
56 individual scale [41], they are still useful to inform strategies at intermediate scales [42, 43, 14, 15, 44].
57 In practice however, a general issue faced by models concerns the comparison of strategies or control
58 measures, in terms of both costs and benefits. In the case of COVID-19 for instance, the computational
59 models mentioned above have considered a wide variety of measures (contact tracing, regular testing,
60 telework, class or school closures), with each study using specific empirical or synthetic data and a
61 specific representation of contacts [17, 20, 45, 46, 22, 19, 47, 48, 49, 21, 44]. However, just as the data
62 representation can affect the identification of risk groups [38], it might also impact the assessment of
63 different strategies. Here we tackle this issue by leveraging high-resolution data describing contacts
64 between individuals in several settings (offices, schools, hospital). We consider several representations
65 of the data, from fine-detailed to coarse-grained ones [38], and use them to inform an agent-based model
66 of SARS-CoV-2 transmission in these settings. We simulate several strategies (reactive and regular
67 testing, telework, reactive class closures) and evaluate their cost and benefit for each representation,
68 highlighting differences and similarities in the outcomes.

69 2 Methods

70 We consider a model for SARS-CoV-2 spread in different settings, namely two schools, an office setting
71 and a hospital ward. In this section, we first present the compartmental model used and the pharma-
72 ceutical (vaccination) and non-pharmaceutical interventions (NPI) considered. We then describe the
73 high-resolution data on interactions between individuals that we use, as well as the hierarchy of coarse-
74 grained representations of the contact patterns that preserve the temporal and structural information
75 of the data at different levels of detail.

76 2.1 Compartmental model

77 We use an agent-based model in which the progression of the disease within each host follows discrete
78 states, as sketched in Figure 1a [20]. Infectious individuals can transmit the disease to susceptible
79 (healthy) individuals (S), who first enter the exposed (non-infectious) state (E) and then a pre-
80 symptomatic infectious state (I_p) after a time τ_E . The pre-symptomatic phase lasts τ_p , after which
81 individuals either evolve into a sub-clinical infection (I_{sc}) or manifest a clinical infection I_c , with
82 respective probabilities $1 - p_c$ and p_c . The infectious state leads finally to the recovered state R after a
83 time τ_I . The disease state durations τ_E , τ_p and τ_I are distributed according to Gamma distributions,
84 with average values and standard deviations given in Table 1 (See also Supplementary Material - SM,
85 Section S1.2.4). We explore in SM Section 2.5.1 a wide range of values of the infectious period $\tau_p + \tau_I$
86 as sensitivity analysis.

Table 1: Parameters of the compartmental model, taken from [20]

SEIR parameter	value
	mean (std) [days]
τ_E	4 (2.3)
τ_p	1.8 (1.8)
τ_I	5 (2.0)
R_0	1.5, 3.0
p_c	0.5
σ	1.0
r_β^p, r_β^{sc}	0.55
r_β^c	1.0

Table 2: Reduction in susceptibility σ , probability of clinical infection p_c and relative infectiousness r_β for children and adolescents, with respect to their values for adults. Taken from [20]

parameter	reduction for children	reduction for adolescents
σ	50 %	25%
p_c	60 %	60%
r_β	27 %	0 %

87 Transmission of the disease can occur upon contact between a susceptible and an infectious (I_p, I_{sc}
 88 or I_c). The probability of transmission per unit of time depends on the product of the transmission
 89 rate β , the relative infectiousness r_β of the infectious individual and the susceptibility σ of the agent.
 90 The parameter β is tuned to obtain a desired specific value for the basic reproductive number R_0 , as
 91 detailed in the SM Section S1.3. The relative infectiousness r_β depends on the compartment of the
 92 infectious individual, with a larger r_β^c value for infectious individuals in the clinical state I_c , and lower
 93 values r_β^p and r_β^{sc} for I_p and I_{sc} (Table 1). It also depends on the age class of the infectious, with
 94 adults and adolescents more infectious than children (Table 2). The susceptibility σ also depends on
 95 the age of the susceptible individual, with adults more susceptible than other groups (adolescents and
 96 children have a susceptibility reduced by respectively 25% and 50% with respect to adults, see Table
 97 2). Finally, the probability to develop a clinical infection is also reduced by 60% for both adolescents
 98 and children.

99 We can further enrich the compartmental model of Figure 1a by considering that individuals can
 100 be vaccinated. Here we do not consider a dynamic vaccination rollout, and assume that vaccination
 101 coverage is fixed throughout the simulation. We also assume full vaccination of individuals. We assume
 102 vaccination to reduce r_β by 50%, σ by 85%, and p_c by 93% We consider (in the SM, Section S2.4)
 103 levels of vaccination coverage of 25%, 50%, and 75%. As sensitivity analysis, we also consider a less
 104 effective vaccine (see SM Section S2.5.4).

105 2.2 Non-pharmaceutical interventions

106 We consider several interventions based on testing and isolation of cases, as well as closure of classes
 107 in school settings, and telework in offices.

108 We use as baseline the protocol of **symptomatic testing and case isolation**: Clinical cases
 109 have a probability $p_D = 0.5$ ($p_D = 0.3$ for children) to take a test and then isolate for $\Delta_Q = 7$ days
 110 after receiving the result of the test. Tests are performed outside work/school hours. Symptomatic

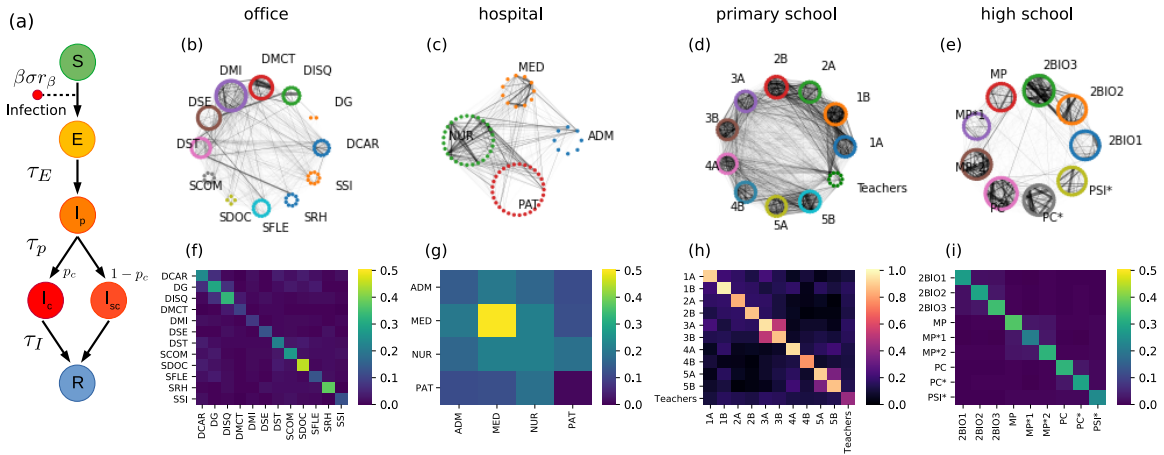


Figure 1: Model and data sets. (a) Schematic illustration of the epidemic model. After contact with an infectious individual, a susceptible individual can become exposed, then transition to a pre-symptomatic state. The individual can then develop either a clinical or a sub-clinical infection before recovering. (b,c,d,e) Weighted networks of contacts for the office, hospital, primary and high school, respectively. For each setting, interactions are aggregated over the first data collection day. The width of an edge is proportional to its weight, i.e., the total contact time between the individuals connected. For each setting, the individuals belonging to the same category are represented in a circle; the categories correspond to: departments in offices, roles in the hospital (doctors, nurses, administrative staff and patients), classes in the school settings. (f,g,h,i) Contact matrices showing the average daily density of links between categories respectively in the offices, hospital, primary school and high school.

111 individuals remain isolated while they wait for their test results. This protocol is used as a reference
112 protocol against which all other protocols are compared.

113 With symptomatic testing and case isolation always implemented, we consider the following addi-
114 tional NPIs:

- 115 • **Regular testing:** Non-vaccinated individuals are periodically tested. We explore weekly, semi-
116 weekly (twice per week) or biweekly (once every two weeks) testing with an adherence α (fraction
117 of the population accepting to get tested). Positive cases remain in isolation for $\Delta_Q = 7$ days.
118 Tests are performed during work/school hours.
- 119 • **Telework:** Telework is implemented only in the office setting. We explore weekly, semiweekly
120 (twice per week) or biweekly (once every two weeks) telework. For each individual, we fix at
121 random the days of the week in which they work remotely and have no contact with the other
122 office workers.
- 123 • **Class quarantine:** This protocol is implemented only in the school settings. When an individual
124 is tested positive upon symptomatic testing, the whole class goes into isolation for $\Delta_Q = 7$ days.
- 125 • **Reactive testing:** This protocol is implemented in the school settings and in the office setting.
126 When an individual tests positive upon symptomatic testing, the non-vaccinated students of the
127 same class (for schools) or the members of the same department (for offices) are tested after a
128 time $\Delta_{r1} = 1$ day, with an adherence α . A second test is performed after $\Delta_{r2} = 4$ days. Positive
129 cases are quarantined during $\Delta_Q = 7$ days.

130 In the office setting, we additionally consider a protocol in which regular testing is combined with
131 telework. Further details of the implementation can be found in the SM Section S1.2.

132 The efficacy of a protocol is quantified in terms of relative reduction of cases with respect to the
133 symptomatic testing protocol at the end of 60 simulation days. The cost is measured as the average
134 number of days spent in quarantine per individual after 60 days. In addition, we measure the number
135 of tests performed after 60 days. Costs and benefits are also evaluated at additional points in time
136 (after 30, 90 or 120 days), see SM Section S2.5.5.

137 In all scenarios, we consider self-administered antigenic tests with turnaround time $\Delta_w = 15$
138 minutes [20]. We assume the tests to have a 100% specificity, and a sensitivity θ which depends on
139 the infectious compartment, with $\theta_p = 0.5$, $\theta_c = 0.8$, and $\theta_{sc} = 0.7$ for the pre-symptomatic, clinical
140 and sub-clinical compartments respectively. As sensitivity analysis, we consider in the SM the case of
141 PCR tests with higher sensitivity and longer turnaround time (see SM Section S2.5.2).

142 2.3 Empirical contact data

143 We use high-resolution face-to-face empirical contacts data collected using wearable sensors in four
144 different settings, two workplaces and two educational contexts: an office building, an hospital, a
145 primary school and a high school. The data sets are publicly available on the website [http://www.
146 sociopatterns.org/datasets](http://www.sociopatterns.org/datasets).

- 147 • The office data set gathers the contacts among 214 individuals, measured in an office building in
148 France during two weeks in 2015 [41]. Individuals are divided in 12 departments with different
149 sizes.
- 150 • The hospital data set describes the interaction among 42 health care workers (HCWs) and 29
151 patients in a hospital ward in Lyon, France, gathered during three days in 2010 [32]. HCWs are
152 divided in three roles: nurses, doctors, and administrative staff.
- 153 • The primary school data set describes the contacts among 232 children and 10 teachers in a
154 primary school in Lyon, France, during two days of school activity in 2009 [42]. The school is
155 composed of 5 grades, each of them comprising 2 classes, for a total of 10 classes; there is a
156 teacher for each class.

157 • The high school data set describes the contacts among 324 students of "classes préparatoires" in
 158 Marseille, France, during one week in 2013 [50]. These classes are located in high schools and are
 159 specific to the French schooling system: they gather students for 2-year studies at the end of the
 160 standard curriculum to prepare for entry exams at specific Universities. Students are grouped
 161 in 9 different classes, and classes are divided in three groups, each focusing on a specialization
 162 (mathematics and physics; physics, chemistry, engineering studies; biology).

163 Data sets are available as lists of contacts over time between anonymized individuals, with a
 164 classification by department (for the office setting), role (for the hospital) or class (for the school
 165 settings), and in terms of students/teachers (for the primary school). From the raw data, we built
 166 the corresponding temporal contact networks, composed of nodes representing individuals, and links
 167 representing empirically measured proximity contacts occurring at a given time (see SM Section S1.1.1).

168 Figure 1b-e displays for each setting a graph of the links aggregated over one day for each data set
 169 (where the weight of a link between two individuals is given by the total contact time between them).
 170 The corresponding contact matrices representing the daily average density of interactions are shown
 171 in Figure 1f-i. In school settings and in offices, contacts occur preferentially within groups [42, 50, 41].

172 2.4 Data representations

173 The empirical data describes contacts at high resolution, giving temporally resolved information on
 174 who has been in contact with whom. These data can be aggregated into representations at different
 175 levels of detail, i.e., retaining only selected features of the empirical temporal contact network while
 176 aggregating over the others.

177 A first type of representations, which we denote by *individual-based representations*, preserve the
 178 empirical structure of the contact network (who has met whom).

179 • **Dynamical network:** Contacts are aggregated into a different weighted graph for each succes-
 180 sive time window of 15 minutes (The weight of a link between two nodes is given by the time in
 181 contact of the two corresponding individuals during this time window). This representation is
 182 the closest to the raw empirical data (that has a temporal resolution of 20 seconds), and will be
 183 considered as the reference against which the other representations will be compared.

184 • **Heterogeneous network:** Contacts measured during the whole data collection are aggregated
 185 into a single weighted network. The weight of a link (i, j) is given by the average daily contact
 186 time between i and j .

187 • In addition, we consider in the SM Section 2 the **daily heterogeneous network representa-**
 188 **tion:** Contacts are aggregated into a different weighted graph for each of the d_{data} days of data
 189 collection. The weight $w_{ij,d}$ of a link (i, j) on day d is given by the total contact time registered
 190 between i and j during the corresponding day.

191 In a second type of representations, the *category-based representations*, we aggregate individuals into
 192 categories, corresponding to departments for the office data, to roles for the hospital data, and to classes
 193 in the school settings (and a category for teachers in the primary school data). Individuals belonging
 194 to a given category are considered as a priori equivalent. For each pair of categories X and Y , we
 195 summarize the interactions between individuals of these categories by the list of daily contact weights
 196 $D_{XY} = \{w_{ij,d} | i \in X, j \in Y, d \in [1, d_{data}]\}$. The average daily number of links between individuals of
 197 categories X and Y is $E_{XY} = |D_{XY}|/d_{data}$, and the quantity $W_{XY} = \sum_{i \in X, j \in Y, d} w_{ij,d}/d_{data}$ gives the
 198 average daily total time in contact between individuals of categories X and Y . We define the three
 199 following data representations based on the concept of contact matrix [38]:

200 • **Contact matrix:** Each individual from category X is connected with all individuals of category
 201 Y with a weight equal to $w_{XY} = W_{XY}/(N_X N_Y)$ (N_X is the number of individuals in category
 202 X ; for $X = Y$ we set $w_{XX} = W_{XX}/(N_X(N_X - 1)/2)$). This representation only retains the

Table 3: Number of days d_{data} of the data set, number of individuals N , initial hour (t_i) and final hour (t_f) of each day, and days of activity in each week (indicated with an X) for each setting.

Setting	d_{data}	N	t_i	t_f	M	T	W	T	F	S	S
offices	10	214	8:00	20:00	X	X	X	X	X		
hospital	3	71	5:00	00:00	X	X	X	X	X	X	X
primary school	2	242	8:30	17:15	X	X		X	X		
high school	4	324	9:00	18:00	X	X	X	X	X		

203 average time spent in contact between members of given categories. For instance in the hospital
 204 data, $W_{NUR,ADM}$ gives the total contact time between nurses and members of the administrative
 205 staff.

206 • **Contact matrix of distributions:** This representation preserves the information about the
 207 density of links between categories and the statistical heterogeneity of the daily contact durations
 208 between pairs of individuals. First, we create for each day a random graph assigning E_{XY} random
 209 links connecting individuals of categories X and Y . The weight of each link between individuals
 210 of categories X and Y is then drawn from a negative binomial distribution, obtained by fitting the
 211 empirical distribution D_{XY} through a maximum likelihood procedure. In the hospital data for
 212 instance, for the contacts between nurses and administrative staff members, this representation
 213 retains the actual average daily number $E_{NUR,ADM}$ of links between these categories, and it also
 214 uses the fitted distribution of all observed daily contact times between nurses and staff members.

215 • In addition, we consider in the SM Section 2 the **contact matrix of bimodal distributions:**
 216 Similarly to the contact matrix of distributions, this representation retains the information about
 217 the density of links between categories, but it disregards the heterogeneity of link weights. We
 218 thus create for each day a graph with E_{XY} random links connecting individuals of categories X
 219 and Y . However, only the average of each distribution D_{XY} is retained: each link is assigned
 220 a weight $\tilde{w}_{XY} = W_{XY}/E_{XY}$. In the hospital data for instance, $\tilde{w}_{NUR,ADM}$ gives the average
 221 contact time on a link between a nurse and a member of the staff.

222 We also consider for reference a very coarse representation informed only by the total daily contact
 223 time:

224 • **Fully connected:** Individuals are all connected with each other. The weight of each link is
 225 equal to the daily contact time averaged over the whole data set $w = \sum_{XY} W_{XY}/(N(N-1)/2)$,
 226 where $N = \sum_X N_X$ is the total number of individuals.

227 Only the dynamical network representation retains information on the temporal evolution of contact
 228 activity along each day. However, we inform all other representations by the office or school hours and
 229 by the alternation of weekdays and week-ends, as reported in Table 3: no contacts occur outside of
 230 these hours. In particular, no contacts occur during the week-ends in the office and school settings.
 231 During the nights, week-ends (and on Wednesdays for the primary school), nodes are thus isolated in
 232 the simulations.

233 2.5 Simulation setup

234 Simulations are initialized at a random time with one exposed individual chosen at random. Simu-
 235 lations then unfold stochastically (see SM Section S1.2), with transmission events occurring, for each
 236 representation, along the contacts available in that representation of the data. To simulate the dis-
 237 ease spreading on longer time scales than the available data (Table 3), copies of the initial data are
 238 repeated over time. Periodic introductions are considered to model infections from community. At
 239 regular intervals a susceptible individual in the considered setting is chosen at random and switched

240 to the exposed compartment (see SM Section S1.2.5). To simulate a limited adherence to testing,
241 the individuals accepting to perform tests are randomly chosen at the beginning of each simulation.
242 Finally, we also explore in the SM Section S2.2 the effect of initial immunity, simulated by the fact that
243 a fraction of the population, randomly chosen at the start of each simulation, cannot be contaminated.

244 As discussed in [38, 39], simulations using a given rate of transmission β performed on different data
245 representations yield different outcomes: less detailed representations tend to yield a higher epidemic
246 final size compared to the dynamical network representation [38], as they make more transmission
247 paths available. Therefore, we fix a target basic reproductive number R_0 in the absence of any control
248 measures and starting with one random seed in an otherwise susceptible population, and calibrate for
249 each representation the rate of transmission β needed to obtain the target R_0 (see SM Section S1.3).

250 We consider two types of simulations. On the one hand, we study the dynamics of the spreading
251 process in the absence of interventions, starting from one random seed and with no introductions, and
252 running simulations until no infectious individual is present in the population (Section 3.1). Results are
253 averaged over 2000 simulations, except the distributions of number of secondary infections for which we
254 use 6000 simulations. On the other hand, to evaluate NPIs, we consider in Section 3.2 simulations of a
255 spread starting from one initial seed, with in addition bi-weekly introductions of exposed individuals.
256 We simulate the spread for 60 days and compute the final epidemic size as well as the number of days
257 that individuals spent in quarantine and the number of tests performed. Each result corresponds to a
258 median over 2000 simulations, with bootstrapped confidence intervals (see SM Section S1.4).

259 3 Results

260 3.1 Unmitigated spread on different data representations

261 We present here the results concerning the unmitigated spread with $R_0 = 3$ in the office data set, and
262 we show in the SM Section S2.2 the results for the other data sets and both $R_0 = 1.5$ and $R_0 = 3$.

263 Figure 2 highlights differences and similarities between the processes taking place on different rep-
264 resentations of the same data set. Figure 2a shows the distributions of the number of secondary cases
265 resulting from one random seed, $R_{0,i}$ (the basic reproductive number R_0 , which takes by construction
266 the same value in all cases, being the average of this distribution), obtained on the various data rep-
267 resentations. All distributions span a rather wide range of values, with events reaching almost four times
268 the average. However, the curves exhibit distinct shapes depending on the type of representation.
269 In the category-based representations, both small and large values of $R_{0,i}$ have a lower probability
270 than for individual-based representations, i.e., both the probability that the spread never starts and
271 the probability that super-spreading events occur are lower. Fitting the distributions with negative
272 binomials yields indeed values of the over-dispersion parameter k larger for the individual-based rep-
273 resentations (≈ 0.5 for $R_0 = 3$ in the office data set, see SM Section S2.2) than for the category-based
274 ones (≈ 0.25 for the contact matrix representations and ≈ 0.22 for the fully connected representation,
275 for $R_0 = 3$ in the office data set, see SM Table S4).

276 Another interesting difference between the two types of representations arises from the investigation
277 of how the spread evolves within the population. Figure 2b shows the temporal behaviour of the fraction
278 of infected individuals for the various representations. The growth is slightly faster at short times for
279 individual-based representations with respect to category-based ones, saturating at earlier times and
280 smaller final epidemic sizes. These differences in dynamics can be understood by examining which
281 nodes are infected at early and late stages of the spread. Indeed, a spreading process on a network
282 tends first to reach the most connected nodes, with a following cascade towards the less connected
283 nodes, so that the average number of neighbours of newly infected nodes decreases with time [51]. Here,
284 as heterogeneities concern contact times rather than numbers of neighbours [35], we show in Figure 2c
285 the average daily strength $\langle s_{new} \rangle (w)$ of individuals who are infected and become exposed during
286 week w (the strength s of an individual is the average daily time in contact with other individuals).
287 The cascading process from individuals with large s towards individuals with lower s is seen as a

288 decreasing trend of $\langle s_{new} \rangle (w)$ for the individual-based representations. For the category-based
 289 representations, the cascade still exists, but the effect is weaker: all individuals within a category are
 290 equivalent, but some categories are more connected than others, so that some heterogeneity remains
 291 in the population. Overall, at early times the newly infected individuals are more connected in the
 292 individual-based representations than in category-based ones, leading to a faster spread. At later times,
 293 the tendency is inverted, with a slower spread on individual-based representations; moreover, as the
 294 remaining susceptible individuals tend to be less well connected, and as less paths are available to reach
 295 them, the final epidemic size is also smaller. On the other hand, simulations using the fully connected
 296 representation cannot show any such effect as all individuals are equivalent. An additional difference is
 297 observed between the heterogeneous network and the dynamical network representations: more causal
 298 propagation paths are present in the heterogeneous network case (where the same network of contacts
 299 is present every day) so that more nodes with smaller strength can be reached by the cascade and a
 300 larger epidemic size is obtained (as seen in Figure 2b).

301 Similar results across representations are obtained considering a partially immune population (SM
 302 Section 2.2).

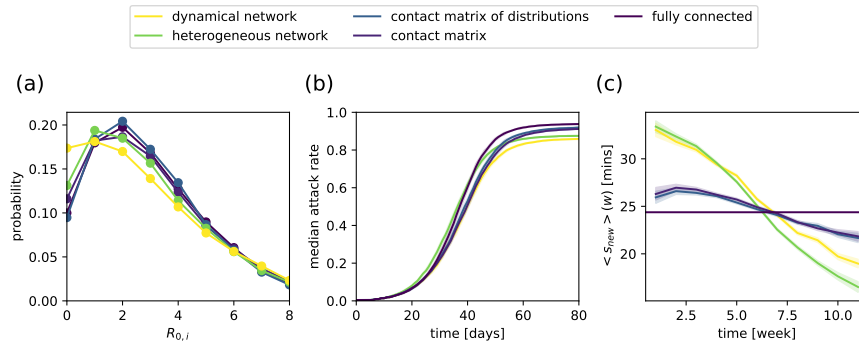


Figure 2: Spreading dynamics on different representations of the office data set, for $R_0 = 3.0$, starting from a single initial exposed seed and no initial immunity. (a) Distribution of the number of secondary infections produced by the initial seed. (b) Temporal evolution of the median attack rate (fraction of individuals who have been infected), starting from one single exposed individual in an otherwise susceptible initial population. (c) Average strength (daily time in contact) of newly infected individuals infected in a given week vs. time. For individual-based representations, a cascade from more connected individuals to less connected ones is observed. The cascade is less pronounced for category-based representations and absent for the fully connected case. Shaded areas correspond to the estimated error, obtained as a bootstrapped CI (see SM Section S1.4).

303 3.2 Robustness of the evaluation of NPIs

304 We show here the results of simulations implementing NPIs for $R_0 = 1.5$, and present additional
 305 results and sensitivity analysis in the SM Sections S2.3-S2.5. We illustrate the numerical simulations
 306 in the Supplementary videos SV1 and SV2: each video shows a single run in the office data set, with
 307 the symptomatic testing protocol (SV1) and the regular testing protocol (SV2, with weekly testing
 308 and 75% adherence). In each video, we present side-by-side runs on three different representations of
 309 the data: the dynamical network, the heterogeneous network and the contact matrix of distributions.
 310 This shows how the links of the dynamical network change at every time step, while the heterogeneous
 311 network links are fixed (disappearing only during nights and weekends) and the links of the contact
 312 matrix of distributions representation are renewed daily.

313 We consider testing and isolation of symptomatic individuals to be the minimal strategy at play,
314 and focus on a comparison of all protocols with respect to this strategy (the impact of this baseline
315 intervention with respect to the absence of intervention is shown in the SM section S2.3). We present
316 the results for the office and primary school data sets in Figure 3, and show the results for other data
317 sets in the SM Section S2.3, as well as additional values of the protocols' parameters. Figure 3a-b
318 shows the reduction in the median epidemic size after 60 days for several protocols, with respect to
319 the symptomatic testing, with protocols ranked in order of increasing reduction. Strikingly, even if the
320 precise values of the efficacy of each protocol depend slightly on the data representation used in the
321 simulations, the ranking of protocols remains almost always the same, both for benefits (Figure 3a,b)
322 and costs (Figure 3c,d). In particular, telework in the offices is particularly efficient, as it reduces the
323 number of contacts of all individuals [19], whereas reactive strategies at school are less efficient than
324 regular testing, because asymptomatic transmissions mostly go undetected, as shown in [20]. These
325 conclusions are reached for all the data representations. Note that the robustness of the ranking with
326 respect to the representation is very strong but not perfect: if two protocols yield very close average
327 efficacy values, one can seem slightly better than the other for one representation and slightly worse
328 for another. Moreover, some exceptions can be observed, such as the case of the fully connected
329 representation, giving a lower efficacy of the reactive testing protocol compared to biweekly regular
330 testing with 25% adherence, while the other representations yield the opposite ranking (see SM Section
331 S2.3.1). Figure 3e-f show that the impact of a protocol on the distributions of epidemic sizes is also
332 similar across representations: here, regular testing yields a strong reduction of the probability of
333 having a large epidemic size and a higher peak at small sizes. We also show in the SM Section S2.3
334 how, when two protocols have similar efficacies, the resulting distributions of epidemic sizes are also
335 very similar, and that this similarity holds across representations.

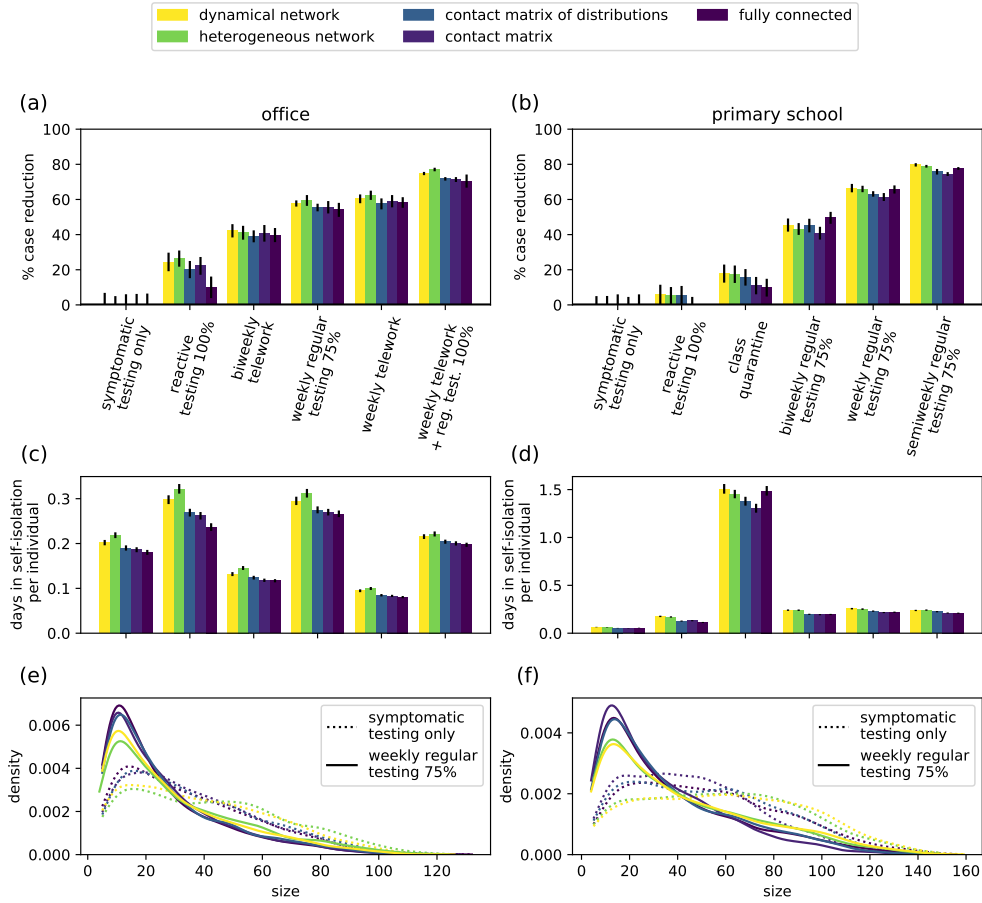


Figure 3: Evaluation of several NPIs in offices and primary school settings, for $R_0 = 1.5$ and simulations performed using different data representations. (a,b) Efficacy of NPIs in offices and primary school, sorted by increasing order of efficacy in the dynamical network representation. Efficacy is defined as the relative reduction in median size compared with symptomatic testing alone, after a period of 60 days. (c,d) Average number of days in quarantine per individual under different protocols (Same x-axis as panels a and b). (e-f) Epidemic size distributions for the symptomatic testing protocol (dotted lines), and for weekly regular testing with 75% adherence (continuous line).

336 We illustrate these results further in Figure 4, where we investigate the question of the adherence
337 to regular testing needed in offices to obtain the same efficacy as telework, for a given testing frequency
338 (Figure 4a). Although the value of the median size reduction obtained by telework slightly depends
339 on the data representation (one day per week of telework yields a $59 \pm 3\%$ and $60 \pm 3\%$ reduction for
340 contact matrix and dynamical network representations, respectively), we estimate that regular testing
341 with the same frequency becomes as efficient as telework for adherence values that remain similar across
342 data representations, ranging from 84% (contact matrix representation) to 81% (dynamical network
343 representation). Figure 4b considers instead the comparison between the regular testing and the class
344 quarantine protocol: the estimation of the adherence needed for regular testing to become more efficient
345 than class quarantine is also consistent across data representations. Another interesting point concerns
346 the effect of increasing the number of tests, either by increasing adherence or by increasing frequency,
347 within the regular testing protocol. First, the increase in efficacy faces diminishing returns (the efficacy
348 grows less fast than proportionally to the number of tests). Second, and as already noted in [20] with
349 simulations on the dynamical network representation of a school data set, increasing adherence has
350 a bigger impact than an increase in frequency (at equal additional number of tests). Figure 4c-d
351 illustrates these points by showing the average size reduction per test for the weekly testing protocol
352 with adherence 50%, and comparing it with the additional size reduction per test obtained for twice
353 the number of tests, obtained either by doubling the adherence at the same frequency, or by doubling
354 the frequency at the same adherence. We show in the SM Section S2.3.3 that this property holds in
355 all settings, and for all data representations.

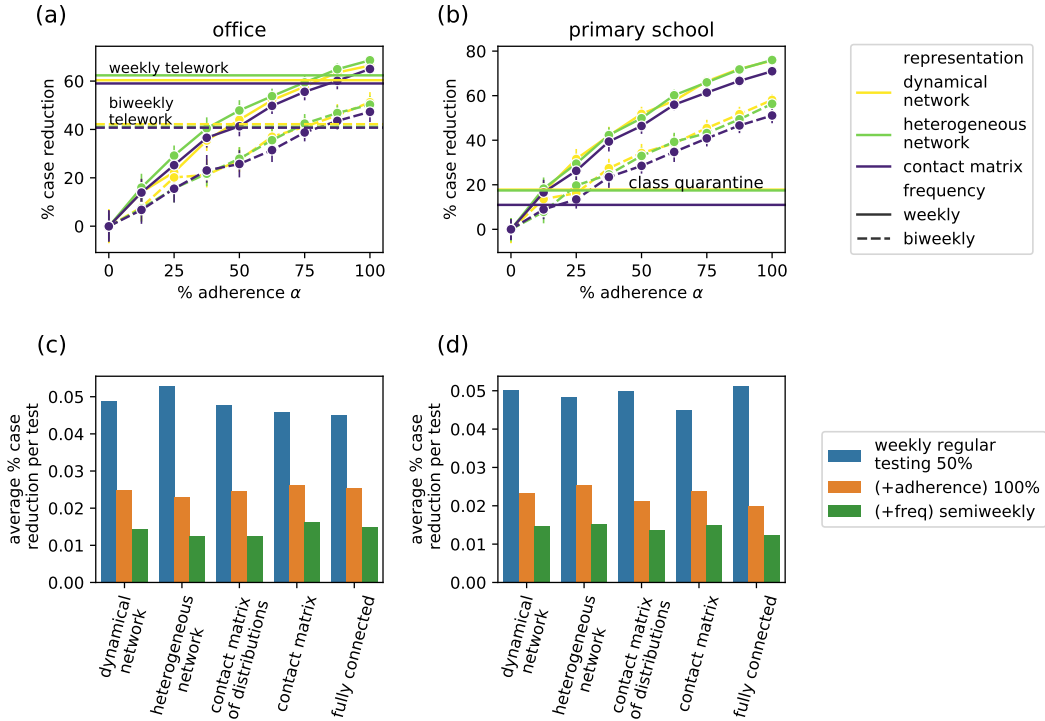


Figure 4: Effect of increasing adherence and frequency in regular testing protocols. (a) Effect of the adherence α for a given frequency (once per week or every two weeks) in the regular testing protocol for the office data set and $R_0 = 1.5$, compared with telework, for several data representations. Horizontal lines correspond to the performance of telework at the same frequencies. (b) Effect of the adherence α for a given frequency (once per week or every two weeks) in the regular testing protocol, compared with the class quarantine protocol, for the school data set and $R_0 = 1.5$. Horizontal lines correspond to the class quarantine protocol. (c,d) Effect of improving adherence or frequency, for $R_0 = 1.5$ for offices (c) and primary school (d). We consider weekly regular testing and $\alpha = 50\%$, and we measure the average size reduction (w.r.t. symptomatic testing) per test (in blue), and the additional size reduction per additional test when doubling the adherence (in orange), and when doubling the frequency (in green).

356 In the SM Section S2.3.2 we examine the impact of the reproductive number R_0 . As also observed
 357 in [20, 48], the efficacy of each protocol depends in a non-monotonic way on R_0 . At small R_0 , even the
 358 symptomatic testing protocol leads to small epidemic sizes, so that additional protocols have a limited
 359 impact. At very large R_0 instead, even the best protocols reach their limits and the spread cannot
 360 be well mitigated. These arguments hold for any data representation, and we indeed observe this
 361 non-monotonicity for all data representations. However, the optimal range of R_0 depends on the data
 362 representation, with a larger value of the optimal R_0 for the category-based representations. Moreover,
 363 the differences between the efficacy values of a given protocol by using different data representations
 364 become larger at large R_0 , with a larger estimated efficacy when using category-based representations.

365 Different protocols have different efficacies but also different costs, which need to be taken into
 366 account in decision making processes. We thus compare in Figure 3c-d the cost of each protocol
 367 simulated on each data representation, computed as the average number of days spent in quarantine
 368 per node. As for the efficacy, the precise evaluation of the cost depends on the data representation,
 369 but the ranking of protocols according to their cost does not (this is also true for the cost in terms

370 of number of tests, as shown in the SM Section 2.3). In particular, regular testing at school avoids a
371 large fraction of the number of days of class lost, with respect to reactive class closures. In the offices,
372 regular testing is more costly than telework, as the latter simply decreases the number of contacts
373 without quarantining individuals.

374 Overall, Figure 3 indicates that a coherent picture of the relative efficacy and cost of different
375 protocols is obtained when using different representations of the data in the numerical simulations,
376 even if quantitative differences in the precise evaluation are observed. Additional results shown in
377 the SM Section S2.5 indicate that these conclusions are robust with respect to changes in disease
378 and protocol parameters: even if the values of the efficacy and costs of each strategy depend on the
379 parameters, and the ranking of strategies can even vary (e.g., for different values of the infectious
380 period), this ranking remains independent of the data representation. We also explore in the SM
381 Section S2.4 the combined effect of NPIs and vaccination. Using any data representation, vaccination
382 alone reduces the final epidemic size even in absence of NPIs or for the symptomatic testing protocol,
383 and decreases the costs in terms of quarantines. Considering vaccination coupled to NPIs, results
384 confirm the robustness of the ranking of protocols, when evaluated in terms of costs and benefits,
385 highlighting the supplementary control that these strategies may have at intermediate vaccination
386 coverages [20, 44].

387 4 Discussion

388 We used high-resolution contact data sets to build aggregated representations and evaluate how loss
389 of resolution informing epidemic models can influence the evaluation of prevention and control strate-
390 gies. Numerical simulations of a model for the spread of SARS-CoV-2 in educational and professional
391 contexts show that detailed representations are needed to correctly account for over-dispersion of re-
392 production numbers and for an accurate evaluation of the efficacy and costs of each strategy. However,
393 coarse representations containing only very summarized information are good enough to rank protocols,
394 and thus to provide insights on better options given the context.

395 Models offer a unique opportunity to evaluate strategies for prevention and control of epidemics,
396 anticipating their expected advantage and costs associated to inform public health decisions. Depend-
397 ing on the context and the question to be addressed, models need to integrate an accurate description
398 of the population under study and of the contacts along which disease transmission occurs. In recent
399 years, the increasing availability of data sets describing contacts between individuals has made it pos-
400 sible to devise models exposing the complexity of human interactions in terms of number of contacts,
401 repeated contacts, frequency, duration, etc. For instance, models integrating data describing interac-
402 tions with high temporal and spatial resolutions can be used to design and study measures tailored
403 to specific contexts such as schools, where repetition of contacts because of friendships and structural
404 organization of contacts due to classes impact the resulting epidemic dynamics [14, 47, 21, 20]. Com-
405 plex models are however data hungry, might be difficult to interpret, and are more time-consuming in
406 terms of development and simulations. Moreover, detailed data are not always available, and data sets
407 in specific settings may provide a narrow vision of the interaction patterns occurring in those contexts
408 that may be difficult to generalize. By loosing some of these specificities, aggregated representations
409 may become more generally applicable.

410 Our results show that some differences emerge in the disease spread simulated on different data
411 representations, even when calibrating the simulations to yield the same basic reproductive numbers.
412 In particular, category-based representations tend to find a lower over-dispersion of the distribution
413 of the reproductive number, and could thus lead to difficulties in correctly estimating the role of
414 superspreading events. This is in line with recent results highlighting the role of contact heterogeneities
415 in superspreading [37]. As they ignore individual differences, these representations cannot inform
416 strategies targeted towards specific individuals, they are also less able to describe the cascading of a
417 spread from individuals with a high connectivity to less well connected ones [51], and differ in the
418 estimation of the final epidemic size [38].

419 The picture is more complex when dealing with the evaluation of control protocols. On the one
420 hand, the ranking of protocols according to their efficacy or their cost does not depend on the data
421 representation. The picture of which protocol is most efficient in each context remains coherent. When
422 a protocol depends on several parameters, the information on which parameter is the most important
423 to act upon is also coherent across data representations (e.g., increasing adherence for regular testing
424 protocols has a larger impact than increasing frequency, at given number of tests). It is even possible to
425 use coarse data representations to quantify the adherence needed for the regular testing to become more
426 efficient than e.g. telework or class quarantine. On the other hand, using various data representations
427 can lead to quantitative differences in the precise values of benefit and cost. This can be a limitation for
428 coarse representations when decisions require accuracy in the estimate of the benefit/cost – for example,
429 to define a minimum benefit that would trigger the application of the measure. Such decisions should
430 thus take into account an inherent uncertainty in the model outcomes due to the limited information
431 contained in the data.

432 We found that regular testing with high enough adherence is a very efficient strategy allowing
433 to limit spread in school contexts while minimizing the number of lost school-days, confirming prior
434 works [20, 52, 21]. In offices, telework is also very efficient [19]. Reactive class closure or reactive
435 testing instead have limited efficacy. The robustness of such results across data representations is
436 explained by the fact that these NPIs reduce the epidemic size through mechanisms that do not depend
437 on the data description. Indeed, the efficacy of reactive measures is limited by the infectiousness of
438 pre-symptomatic and asymptomatic individuals: for instance, due to the resulting silent propagation,
439 many other classes can already have been reached by the infection when one class is closed upon the
440 detection of a case at school [20]. In contrast, regular testing is a proactive approach that allows to
441 detect also pre-symptomatic and asymptomatic cases. Telework on the other side simply reduces the
442 time in contact, reducing the probability of contagion events whatever the data representation. Overall,
443 our results support the use of even coarse representations of the interactions between individuals in
444 settings such as schools or workplaces when evaluating NPIs and potentially choosing between possible
445 protocols.

446 Individual data such as the ones used in this study across different settings are rarely available.
447 Moreover, the existing data sets are each specific to a context and potentially to the time of the
448 data collection campaign. In emergency situations or during a crisis such as the current pandemic,
449 gathering such data in real time encounters many challenges, and more coarse-grained representations
450 are generally opted for. Indeed, summarized data is more accessible, and can be enriched by some
451 robust statistical features of contact data, such as the heterogeneities in contact durations [30, 38,
452 43, 35]. In particular, the division of a population into categories with e.g. different mixing patterns
453 and/or schedules can be performed from limited information such as the existence of classes in a school
454 or of departments in offices. A population can also be separated in groups according to an expected
455 diversity of behaviours, as for instance in [44] that singles out the group of "more social" students in a
456 US campus as the ones belonging to fraternities and shows that targeted testing of this category can
457 be an efficient strategy.

458 Our work comes with several limitations. First, the data we used describe contacts collected during
459 only few days. Here, we have used the simplest method of repeating the data set in order to simulate the
460 contacts in the population during an extended time, whereas contacts are not repeated identically in the
461 real world. However, the simulations performed in [20] used different ways of artificially extending the
462 data duration and found no differences in the results. The settings we have considered are also relatively
463 small, but represent the state of the art in terms of data describing interactions between individuals, and
464 have very different structural and temporal properties because of structure and activities performed.
465 More work needs to be done to generate synthetic data sets at such resolution in larger settings. Second,
466 we used a rather simple coupling with the community, through regular introduction of cases, as the
467 data we considered do not include contacts occurring outside of the studied context. This implies that
468 we do not evaluate the impact of the interventions on the community: different approaches would be
469 needed for this purpose [22, 53], which however would lose resolution within each setting. Without
470 going to such large-scale agent-based models, a possible improvement would be to inform the model

471 with empirical data on the contacts that individuals have with members of the community, or with
472 one another outside of school. Third, we have here considered one specific infectious disease. However,
473 our results are robust with respect to variations in the basic reproductive number, initial immunity,
474 and the impact of vaccination. We have also explored a wide range of possible infectious periods,
475 finding that it can affect the efficacy of measures and even their ranking, but that the ranking remains
476 independent on data representation, at fixed infectious period (as already noted in [6, 38], the precise
477 order of contacts could affect the results for very fast processes whose timescales are of the same order
478 as the temporal resolution). Moreover, SARS-CoV-2 is of particular interest both practically and
479 theoretically, as the pre-symptomatic and asymptomatic transmissions make it necessary to go beyond
480 the usual reactive strategies and to evaluate a range of protocols.

481 Our modelling approaches are agent-based, as the simulations consider distinguishable agents even
482 when the data representations are category-based, which suggests two lines of further research. On the
483 one hand, it would be interesting to extend our results to compartmental models. Indeed, the epidemic
484 curves obtained in a free-spreading scenario by agent-based models and compartmental models can be
485 mapped onto one another upon appropriate recalibration of parameters [40]. However, whether this
486 remains the case when interventions are in place is an open question. On the other hand, the agent-
487 based models we considered deal with the interactions between individuals but do not address the issue
488 of individual heterogeneities with respect to the disease transmission (beyond the differences between
489 children, adolescents, adults), such as heterogeneous infectious periods [54] or heterogeneous rates
490 of transmission [55], nor with respect to potential changes of behaviour depending on the epidemic
491 situation [56]. An interesting extension of this work would be to consider situations where these
492 differences between individuals are correlated with their contact behaviour: to take into account such
493 correlations, one would need to go beyond the category-based representations we have considered here,
494 allowing heterogeneous properties within each category, in the spirit of degree-corrected stochastic
495 block models [57].

496 Acknowledgments

497 This study was partially funded by: ANR projects COSCREEN (ANR-21-CO16-0005) and DATARE-
498 DUX (ANR-19-CE46-0008-03); ANRS-MIE project EMERGEN (ANRS0151); EU H2020 grants MOOD
499 (H2020-874850) and RECOVER (H2020-101003589); EU HORIZON grant VERDI (101045989).

500 References

- 501 [1] Roy M Anderson and Robert M May. Infectious diseases of humans: dynamics and control. Oxford
502 university press, 1992.
- 503 [2] Matt J Keeling and Pejman Rohani. Modeling infectious diseases in humans and animals. Prince-
504 ton University Press, 2011.
- 505 [3] D. Balcan, V. Colizza, B. Gonçalves, H. Hu, J.J. Ramasco, and A. Vespignani. Multiscale mobility
506 networks and the spatial spreading of infectious diseases. Proc Natl Acad Sci USA, 106:21484–
507 21489, 2009.
- 508 [4] V. Colizza, A. Barrat, M. Barthelemy, A.-J. Valleron, and A. Vespignani. Modeling the worldwide
509 spread of pandemic influenza: Baseline case and containment interventions. PLOS Medicine,
510 4(1):e13, 2007.
- 511 [5] Neil M. Ferguson, Derek A. T. Cummings, Christophe Fraser, James C. Cajka, Philip C. Cooley,
512 and Donald S. Burke. Strategies for mitigating an influenza pandemic. Nature, 442(7101):448–452,
513 2006.

- 514 [6] Juliette Stehlé, Nicolas Voirin, Alain Barrat, Ciro Cattuto, Vittoria Colizza, Lorenzo Isella,
515 Corinne Régis, Jean-Francois Pinton, Nagham Khanafer, Wouter Van den Broeck, and Philippe
516 Vanhems. Simulation of an seir infectious disease model on the dynamic contact network of
517 conference attendees. *BMC Medicine*, 9(1):87, 2011.
- 518 [7] M. Tizzoni, P. Bajardi, C. Poletto, J.J. Ramasco, D. Balcan, B. Goncalves, N. Perra, V. Colizza,
519 and A. Vespignani. Real-time numerical forecast of global epidemic spreading: case study of 2009
520 a/h1n1pdm. *BMC Medicine*, 10:165, 2012.
- 521 [8] Matteo Chinazzi, Jessica T. Davis, Marco Ajelli, Corrado Gioannini, Maria Litvinova, Stefano
522 Merler, Ana Pastore y Piontti, Kunpeng Mu, Luca Rossi, Kaiyuan Sun, Cécile Viboud, Xinyue
523 Xiong, Hongjie Yu, M. Elizabeth Halloran, Ira M. Longini, and Alessandro Vespignani. The effect
524 of travel restrictions on the spread of the 2019 novel coronavirus (covid-19) outbreak. *Science*,
525 368(6489):395–400, 2020.
- 526 [9] Giulia Pullano, Francesco Pinotti, Eugenio Valdano, Pierre-Yves Boëlle, Chiara Poletto, and
527 Vittoria Colizza. Novel coronavirus (2019-ncov) early-stage importation risk to europe, january
528 2020. *Eurosurveillance*, 25(4), 2020.
- 529 [10] Laura Di Domenico, Giulia Pullano, Chiara E Sabbatini, Pierre-Yves Boëlle, and Vittoria Colizza.
530 Impact of lockdown on covid-19 epidemic in ile-de-france and possible exit strategies. *BMC*
531 *medicine*, 18(1):1–13, 2020.
- 532 [11] Moritz U. G. Kraemer, Chia-Hung Yang, Bernardo Gutierrez, Chieh-Hsi Wu, Brennan Klein,
533 David M. Pigott, null null, Louis du Plessis, Nuno R. Faria, Ruoran Li, William P. Hanage, John S.
534 Brownstein, Maylis Layan, Alessandro Vespignani, Huaiyu Tian, Christopher Dye, Oliver G.
535 Pybus, and Samuel V. Scarpino. The effect of human mobility and control measures on the
536 covid-19 epidemic in China. *Science*, 368(6490):493–497, 2020.
- 537 [12] Juanjuan Zhang, Maria Litvinova, Yuxia Liang, Yan Wang, Wei Wang, Shanlu Zhao, Qianhui
538 Wu, Stefano Merler, Cécile Viboud, Alessandro Vespignani, et al. Changes in contact patterns
539 shape the dynamics of the COVID-19 outbreak in China. *Science*, 368(6498):1481–1486, 2020.
- 540 [13] Laura Di Domenico, Chiara E Sabbatini, Giulia Pullano, Daniel Lévy-Bruhl, and Vittoria
541 Colizza. Impact of january 2021 curfew measures on sars-cov-2 b.1.1.7 circulation in france.
542 *Eurosurveillance*, 26(15), 2021.
- 543 [14] Valerio Gemmetto, Alain Barrat, and Ciro Cattuto. Mitigation of infectious disease at school:
544 Targeted class closure vs school closure. *BMC Infectious Diseases*, 14(1):1–10, 2014.
- 545 [15] Constanze Ciavarella, Laura Fumanelli, Stefano Merler, Ciro Cattuto, and Marco Ajelli. School
546 closure policies at municipality level for mitigating influenza spread: a model-based evaluation.
547 *BMC Infectious Diseases*, 16(1):576, 2016.
- 548 [16] Joel R Koo, Alex R Cook, Minah Park, Yinxiaohe Sun, Haoyang Sun, Jue Tao Lim, Clarence
549 Tam, and Borame L Dickens. Interventions to mitigate early spread of sars-cov-2 in singapore: a
550 modelling study. *The Lancet Infectious Diseases*, 20(6):678–688, 2020.
- 551 [17] Adam J Kucharski, Petra Klepac, Andrew JK Conlan, Stephen M Kissler, Maria L Tang, Hannah
552 Fry, Julia R Gog, W John Edmunds, Jon C Emery, Graham Medley, et al. Effectiveness of
553 isolation, testing, contact tracing, and physical distancing on reducing transmission of sars-cov-2 in
554 different settings: a mathematical modelling study. *The Lancet Infectious Diseases*, 20(10):1151–
555 1160, 2020.

- 556 [18] David R. M. Smith, Audrey Duval, Koen B. Pouwels, Didier Guillemot, Jérôme Fernandes, Bich-
557 Tram Huynh, Laura Temime, Lulla Opatowski, and on behalf of the AP-HP/Universities/Inserm
558 COVID-19 research collaboration. Optimizing covid-19 surveillance in long-term care facilities: a
559 modelling study. *BMC Medicine*, 18(1):386, 2020.
- 560 [19] Simon Mauras, Vincent Cohen-Addad, Guillaume Duboc, Max Dupré la Tour, Paolo Frasca, Claire
561 Mathieu, Lulla Opatowski, and Laurent Viennot. Mitigating covid-19 outbreaks in workplaces
562 and schools by hybrid telecommuting. *PLOS Computational Biology*, 17(8):1–24, 08 2021.
- 563 [20] Elisabetta Colosi, Giulia Bassignana, Diego Andrés Contreras, Canelle Poirier, Simon Cauchemez,
564 Yazdan Yazdanpanah, Bruno Lina, Arnaud Fontanet, Alain Barrat, and Vittoria Colizza. Self-
565 testing and vaccination against covid-19 to minimize school closure. *Lancet Inf. Diseases*, 2022.
- 566 [21] Ryan Seamus McGee, Julian R. Homburger, Hannah E. Williams, Carl T. Bergstrom, and Ali-
567 cia Y. Zhou. Model-driven mitigation measures for reopening schools during the covid-19 pan-
568 demic. *Proceedings of the National Academy of Sciences*, 118(39), 2021.
- 569 [22] Quan-Hui Liu, Juanjuan Zhang, Cheng Peng, Maria Litvinova, Shudong Huang, Piero Po-
570 letti, Filippo Trentini, Giorgio Guzzetta, Valentina Marziano, Tao Zhou, Cecile Viboud, Ana I.
571 Bento, Jiancheng Lv, Alessandro Vespignani, Stefano Merler, Hongjie Yu, and Marco Ajelli.
572 Model-based evaluation of alternative reactive class closure strategies against covid-19. *Nature*
573 *Communications*, 13(1):322, 2022.
- 574 [23] J. Mossong, N. Hens, M. Jit, P. Beutels, K. Auranen, R. Mikolajczyk, M. Massari, S. Salmaso,
575 G. Scalia Tomba, J. Wallinga, J. Heijne, M. Sadkowska-Todys, M. Rosinska, and W.J. Ed-
576 munds. Social Contacts and Mixing Patterns Relevant to the Spread of Infectious Diseases.
577 *PLoS Medicine*, 5(3):e74, 2008.
- 578 [24] Romualdo Pastor-Satorras, Claudio Castellano, Piet Van Mieghem, and Alessandro Vespignani.
579 Epidemic processes in complex networks. *Rev. Mod. Phys.*, 87:925–979, Aug 2015.
- 580 [25] K. Eames, S. Bansal, S. Frost, and S. Riley. Six challenges in measuring contact networks for use
581 in modelling. *Epidemics*, 10:72–77, 2015. Challenges in Modelling Infectious Disease Dynamics.
- 582 [26] Naoki Masuda and Petter Holme, editors. *Temporal Network Epidemiology*. Springer, Singapore,
583 2017.
- 584 [27] J. Wallinga, P. Teunis, and M. Kretzschmar. Using data on social contacts to estimate age-specific
585 transmission parameters for respiratory-spread infectious agents. *Am J Epidemiol*, 164:936–944,
586 2006.
- 587 [28] Jonathan M Read, Ken TD Eames, and W John Edmunds. Dynamic social networks and the im-
588 plications for the spread of infectious disease. *Journal of The Royal Society Interface*, 5(26):1001–
589 1007, 2008.
- 590 [29] Leon Danon, Jonathan M. Read, Thomas A. House, Matthew C. Vernon, and Matt J. Keeling.
591 Social encounter networks: characterizing great britain. *Proceedings of the Royal Society B:*
592 *Biological Sciences*, 280(1765), 2013.
- 593 [30] Ciro Cattuto, Wouter Van den Broeck, Alain Barrat, Vittoria Colizza, Jean-François Pinton, and
594 Alessandro Vespignani. Dynamics of person-to-person interactions from distributed rfid sensor
595 networks. *PLoS ONE*, 5(7):e11596, 07 2010.
- 596 [31] Marcel Salathé, Maria Kazandjieva, Jung Woo Lee, Philip Levis, Marcus W. Feldman, and
597 James H. Jones. A high-resolution human contact network for infectious disease transmission.
598 *Proceedings of the National Academy of Sciences*, 107(51):22020–22025, 2010.

- 599 [32] Philippe Vanhems, Alain Barrat, Ciro Cattuto, Jean François Pinton, Nagham Khanafer, Corinne
600 Régis, Byeul a. Kim, Brigitte Comte, and Nicolas Voirin. Estimating potential infection trans-
601 mission routes in hospital wards using wearable proximity sensors. PloS one, 8(9), 2013.
- 602 [33] Arkadiusz Stopczynski, Vedran Sekara, Piotr Sapiezynski, Andrea Cuttone, Mette My Madsen,
603 Jakob Eg Larsen, and Sune Lehmann. Measuring large-scale social networks with high resolution.
604 PLoS ONE, 9(4):e95978, 04 2014.
- 605 [34] Damon J. A. Toth, Molly Leecaster, Warren B. P. Pettey, Adi V. Gundlapalli, Hongjiang Gao,
606 Jeanette J. Rainey, Amra Uzicanin, and Matthew H. Samore. The role of heterogeneity in contact
607 timing and duration in network models of influenza spread in schools. Journal of The Royal Society
608 Interface, 12(108), 2015.
- 609 [35] Alain Barrat and Ciro Cattuto. Face-to-Face Interactions, pages 37–57. Springer International
610 Publishing, Cham, 2015.
- 611 [36] Sally Blower and Myong-Hyun Go. The importance of including dynamic social networks when
612 modeling epidemics of airborne infections: does increasing complexity increase accuracy? BMC
613 medicine, 9(1):1–3, 2011.
- 614 [37] Zachary Susswein and Shweta Bansal. Characterizing superspreading of sars-cov-2 : from mech-
615 anism to measurement. medRxiv, 2020.
- 616 [38] Anna Machens, Francesco Gesualdo, Caterina Rizzo, Alberto E. Tozzi, Alain Barrat, and Ciro
617 Cattuto. An infectious disease model on empirical networks of human contact: bridging the gap
618 between dynamic network data and contact matrices. BMC Infectious Diseases, 13(1):1–18, 2013.
- 619 [39] Alberto Aleta, Guilherme Ferraz de Arruda, and Yamir Moreno. Data-driven contact structures:
620 From homogeneous mixing to multilayer networks. PLoS computational biology, 16(7):e1008035,
621 2020.
- 622 [40] Livio Bioglio, Mathieu Génois, Christian L. Vestergaard, Chiara Poletto, Alain Barrat, and Vit-
623 toria Colizza. Recalibrating disease parameters for increasing realism in modeling epidemics in
624 closed settings. BMC Infectious Diseases, 16(1):1–15, 2016.
- 625 [41] Mathieu Génois and Alain Barrat. Can co-location be used as a proxy for face-to-face contacts?
626 EPJ Data Science, 7(1):1–18, 2018.
- 627 [42] Juliette Stehlé, Nicolas Voirin, Alain Barrat, Ciro Cattuto, Lorenzo Isella, Jean-François Pinton,
628 Marco Quaghiotto, Wouter Van den Broeck, Corinne Régis, Bruno Lina, et al. High-resolution
629 measurements of face-to-face contact patterns in a primary school. PloS one, 6(8):e23176, 2011.
- 630 [43] Timo Smieszek and Marcel Salathé. A low-cost method to assess the epidemiological importance
631 of individuals in controlling infectious disease outbreaks. BMC medicine, 11(1):1–8, 2013.
- 632 [44] Peter I. Frazier, J. Massey Cashore, Ning Duan, Shane G. Henderson, Alyf Janmohamed, Brian
633 Liu, David B. Shmoys, Jiayue Wan, and Yujia Zhang. Modeling for COVID-19 college reopening
634 decisions: Cornell, a case study. Proceedings of the National Academy of Sciences, 119(2), 2022.
- 635 [45] Christopher M. Baker, Iadine Chades, Jodie McVernon, Andrew P. Robinson, and Howard Bon-
636 dell. Optimal allocation of pcr tests to minimise disease transmission through contact tracing and
637 quarantine. Epidemics, 37:100503, 2021.
- 638 [46] Laura Di Domenico, Giulia Pullano, Chiara E Sabbatini, Pierre-Yves Boëlle, and Vittoria Colizza.
639 Modelling safe protocols for reopening schools during the covid-19 pandemic in france. Nature
640 communications, 12(1):1–10, 2021.

- 641 [47] Jana Lasser, Johannes Sorger, Lukas Richter, Stefan Thurner, Daniela Schmid, and Peter Klimek.
642 Assessing the impact of sars-cov-2 prevention measures in austrian schools using agent-based
643 simulations and cluster tracing data. Nature Communications, 13(1):554, 2022.
- 644 [48] A. Barrat, C. Cattuto, M. Kivelä, S. Lehmann, and J. Saramäki. Effect of manual and digital
645 contact tracing on COVID-19 outbreaks: A study on empirical contact data. Journal of the Royal
646 Society Interface, 18(178), 2021.
- 647 [49] Jesús A. Moreno López, Beatriz Arregui García, Piotr Bentkowski, Livio Bioglio, Francesco
648 Pinotti, Pierre-Yves Boëlle, Alain Barrat, Vittoria Colizza, and Chiara Poletto. Anatomy of
649 digital contact tracing: Role of age, transmission setting, adoption, and case detection. Science
650 Advances, 7(15):eabd8750, 2021.
- 651 [50] Rossana Mastrandrea, Julie Fournet, and Alain Barrat. Contact patterns in a high school: a
652 comparison between data collected using wearable sensors, contact diaries and friendship surveys.
653 PloS one, 10(9):e0136497, 2015.
- 654 [51] Marc Barthélemy, Alain Barrat, Romualdo Pastor-Satorras, and Alessandro Vespignani. Dynam-
655 ical patterns of epidemic outbreaks in complex heterogeneous networks. Journal of theoretical
656 biology, 235(2):275–288, 2005.
- 657 [52] Ryan Seamus McGee, Julian R Homburger, Hannah E Williams, Carl T Bergstrom, and Alicia Y
658 Zhou. Proactive covid-19 testing in a partially vaccinated population. medRxiv, 2021.
- 659 [53] Benjamin Faucher, Rania Assab, Jonathan Roux, Daniel Levy-Bruhl, Cécile Tran Kiem, Simon
660 Cauchemez, Laura Zanetti, Vittoria Colizza, Pierre-Yves Boëlle, and Chiara Poletto. Agent-
661 based modelling of reactive vaccination of workplaces and schools against covid-19. Nature
662 Communications, 13(1):1414, 2022.
- 663 [54] Alexandre Darbon, Davide Colombi, Eugenio Valdano, Lara Savini, Armando Giovannini, and
664 Vittoria Colizza. Disease persistence on temporal contact networks accounting for heterogeneous
665 infectious periods. Royal Society open science, 6(1):181404, 2019.
- 666 [55] Hui Yang, Ming Tang, and Thilo Gross. Large epidemic thresholds emerge in heterogeneous
667 networks of heterogeneous nodes. Scientific reports, 5(1):1–12, 2015.
- 668 [56] Sebastian Funk, Shweta Bansal, Chris T. Bauch, Ken T.D. Eames, W. John Edmunds, Alison P.
669 Galvani, and Petra Klepac. Nine challenges in incorporating the dynamics of behaviour in in-
670 fectious diseases models. Epidemics, 10:21–25, 2015. Challenges in Modelling Infectious Disease
671 Dynamics.
- 672 [57] Tiago P. Peixoto. Model selection and hypothesis testing for large-scale network models with
673 overlapping groups. Phys. Rev. X, 5:011033, Mar 2015.